23

Downburst Monitoring and Prediction Studies

Kenneth L. Pryor

NOAA/NESDIS Center for Satellite Applications and Research (STAR), College Park, Maryland, USA

Abstract:

Downbursts are defined as convective wind gusts upwards of 50 knots. Mesoscale convective systems (MCS) frequently produce strong downbursts that can cause widespread power outages, tree and structural damage, and transportation accidents that affect multi-state regions and metropolitan areas along their track. A derecho, defined as a long-lived, widespread severe convective windstorm, is composed of numerous downbursts (intense localized storm downdrafts) organized into clusters or families of clusters. Derechos can produce winds above hurricane force along a track that may exceed several hundred kilometers. This chapter shows how ground and satellite-based instrumentation can be combined to monitor windstorms over the American Midwest and Atlantic coastal region.

Convective windstorm potential has been expressed as a grouping of stability parameters that are relevant for downburst generation. These include the lower-to-mid-tropospheric temperature and equivalent potential temperature (theta-e) lapse rates, vertical relative humidity differences, and the amount of convective available potential energy (CAPE) in the troposphere. Accordingly, this chapter will provide background on convective windstorms and a three-step process that monitors the ambient environment that leads to the formation of severe storms and the specific characteristics of those that produce downburst winds. We found that downburst monitoring and subsequent prediction is essentially a three-step process with an objective to build a three-dimensional model of the thermodynamic structure of the ambient environment and conceptual model of downburst-producing convective storms. Collection and exploitation of surface-based observations, ground-based microwave and radio profiler measurements, and satellite-based 2-D plan view images all serve as building blocks in the conceptual modelling process. Modification of sounding profiles with surface observations of temperature and humidity is an additional step that results in improved representation of the ambient environment.

Key Words: Convective storms, windstorms, downbursts, satellite soundings, radiosondes, RADAR

"And suddenly a sound came from heaven like the rush of a mighty wind, and it filled all the house where they were sitting." Acts 2:2 Revised Standard Version Bible

1 Introduction

Downbursts are strong downdrafts that induce an outburst of damaging winds at or near the ground, and a microburst as a very small downburst with an outflow diameter of less than 4 km and a lifetime of less than 5 minutes (Fujita 1985; Wakimoto 1985). The dangers posed by convective storm-generated downbursts have been extensively documented. Since 2000, the National Transportation Safety Board (NTSB) has recorded 48 downburst-related accidents over CONUS with 42 fatalities (National Transportation Safety Board 2021) that involved personal or instructional aircraft. Severe windstorms (i.e., widespread convective wind gusts > 25.7 m s^{-1} (50 kt)) resulting from mesoscale convective systems (MCS) cause significant disruption to society, including widespread power outages, tree and structural damage, and transportation accidents that affect multi-state regions and metropolitan areas along their track. Among them, a derecho, defined as a long-lived, widespread severe convective windstorm, is composed of numerous downbursts that are organized into clusters or families of clusters. Derechos can produce winds above hurricane force along a track that may exceed several hundred kilometers. Between 1987 and 2002, severe convective windstorms resulted in a total property loss of over $3 billion in the United States, with an average loss per event of $96 million. Also, between 1986 and 2003, severe convective windstorms were responsible for a total of 153 deaths and 2605 injuries, proving to be more deadly and hazardous than the low-end (F-0/F-1 intensity) tornado outbreaks that occurred during the same period and resulted in only 71 deaths (Ashley and Mote 2005). Because these events are severe, it is important to understand the factors that lead to the downbursts and utilize all available observations to monitor and forecast their development.

Convective windstorm potential has been traditionally expressed as a grouping of stability parameters relevant for downburst generation. These include the lower-to-mid-tropospheric temperature and equivalent potential temperature (theta-e) lapse rates, vertical relative humidity differences, and the amount of convective available potential energy (CAPE) in the troposphere. Some factors increase the likelihood of severe convective winds, which are (1) an elevated mixed layer that promotes instability by generating powerful storm updrafts and downdrafts (Banacos and Ekster 2010) and (2) a rear-inflow jet into an MCS (Smull and Houze 1987; Weisman 1992) which channels unsaturated mid-tropospheric air into the leading convective storm line. The establishment of an elevated, ascending front-to-rear flow originating from deep, moist convection, overlying a strong and deep outflow-induced cold pool has been found to generate and sustain a robust rear inflow jet (Weisman 1992). Other factors can reduce the likelihood of severe convective winds, such as the presence of a lower-tropospheric temperature inversion and a surface-based layer of unsaturated air that reduces virtual temperature.

Meteorological satellite measurement data, especially brightness temperature measured at the surface and convective cloud tops, has been previously exploited to study the troposphere's thermodynamic structure and convective storms' physical structure. Fujita and Wakimoto ("FW," 1981) demonstrated one of the earliest studies that identified infrared imagery from geostationary satellites showing definite cloud-top signatures associated with large and robust downbursts on the ground. Ellrod (1989) first applied geostationary sounder instrument data to the study of downburst potential assessment for

the 2 August 1985 Dallas-Ft. Worth (DFW), Texas microburst storm. Since then, new technology and instrumentation have improved monitoring severe windstorms.

This chapter presents a discussion of the science of operational forecasting of severe windstorms through examples of employing new satellite and ground-based microwave and vertical wind profile data. Accordingly, this chapter is organized as follows: Section 2 is a detailed background of severe convective windstorm theory that includes a discussion of windstorm genesis and evolution. Section 3 is a summary of instrumentation and measurement application methodology. Finally, as an example of the coordinated use of surface- and satellite-based observational instrumentation, section 4 presents case studies of downburst events from local to regional scale. The objective of this instruction is to build a multi-step procedure for operational convective storm downburst monitoring and prediction.

2 Theoretical Background of Severe Convective Windstorms: Genesis and Evolution

The outline of convective windstorm theory begins with the requirement that severe storms are highly organized. Construction of a model of severe convective winds from a simplified vertical momentum equation is derived from Newton's 2nd Law and expressed in equations 1a) and 1b):

$$a = F/m = (-1/\rho)(dp/dz) + g(T_{ve} - T_{vp})/T_{ve} \quad (1a)$$

$$a = F/m = (-1/\rho)(dp/dz) + g(\rho_o - \rho_f)/\rho_o \quad (1b)$$

where a is the acceleration, ρ is the density of the medium, p is pressure, z is the altitude in the atmosphere, and T_{ve} and T_{vp} are virtual temperatures of the environment (atmosphere) and the parcel, respectively.

Downdraft initiation proceeds as a departure from hydrostatic equilibrium. For a volume of air with a high concentration of ice phase precipitation that develops within a convective storm, the resultant force F on the precipitation volume is downward and imparts negative buoyancy. This physical basis can be extended to more complex convective systems in which updrafts, downdrafts, and outflow foster a rear inflow jet's development.

The standard NOAA/National Weather Service (NWS) definition of a severe thunderstorm includes damaging winds with gusts of 26 m s^{-1} (50 kt) or greater and hail with a diameter of 2.5 cm (1 inch) or greater. Severe thunderstorms are most identifiable in weather radar imagery, in which a large concentration of ice-phase precipitation within a volume results in high reflectivity resulting from increased backscattering. Downdraft severity is governed by phase change and the loading of ice-phase precipitation. Loading, in effect, refers to the mass of a collection of hydrometeors. When gravity is imposed upon the volume of hydrometeors, downward acceleration occurs due to precipitation's weight.

Numerous studies through the 1980s and 1990s provided observational analyses and conceptual models for severe convective wind generation that addressed environmental and storm microphysical and dynamic attributes. A prototypical conceptual model of a deep moist convective (DMC) storm is shown in Figure 1a. Fujita and Wakimoto ("FW," 1981) noted that damaging winds induced by thunderstorms were classified into a tornado

and straight-line winds and further identified a sub-classification of straight-line winds into two categories: the downburst and the gust-front. FW formulated the definition of the downburst as stated at the beginning of Section 1. This study identified that infrared imagery from geostationary satellites showed definite cloud-top signatures associated with large and strong downbursts on the ground.

Srivastava (1987) found that precipitation in the form of ice increases the convective downdraft intensity. This effect increases with precipitation content and the stability of the environmental lapse rate of temperature. The power of the downdraft also increases in proportion to the relative concentration of smaller particles. Condensate loading (Srivastava 1987), sometimes combined with subsaturated air entrainment in the storm middle level (Knupp 1989), initiates the convective downdraft. The subsequent melting of frozen hydrometeors and subcloud evaporation of liquid precipitation, in conjunction with precipitation loading, result in the cooling and negative buoyancy that accelerate the downdraft in the unsaturated layer (Srivastava 1987). The melting of ice-phase precipitation, subsequent evaporative cooling, and the resulting downdraft strength are enhanced by sizeable liquid water content and the related water surface available for evaporation. A large lapse rate maintains negative buoyancy as the downdraft descends in the subcloud layer (Srivastava 1987). As the lapse rate's stability is increased, higher precipitation contents, precipitation in the form of ice, and relatively higher concentrations of small precipitation particles are required to force an intense downdraft. At this point in the downdraft initiation process, potential energy resulting from temperature deficit between the precipitation-infused parcel and the ambient environment is converted to

downward air parcel motion, which, collectively, comprises the convective downdraft. As the lapse rate becomes even more stable, only wet downbursts having substantial precipitation in the form of ice are possible. A downburst can be driven solely below the cloud base where melting and evaporation of precipitation and precipitation loading below the cloud base were sufficient to produce wet downbursts.

Knupp (1989, 1996) refined the understanding of the downburst generation's physical and dynamic processes. The author noted that low-level downdrafts are closely controlled by the arrival of precipitation at low levels. In the storm middle levels, air flows quasi-horizontally around the updraft flanks and converges into the downshear flank, referred to as the wake. Within the wake region, where entrainment reduces positive buoyancy and associated updraft strength, precipitation at middle levels (where it is grown most effectively) is then allowed to descend to lower levels. The intrusion of drier air into the wake's precipitation region also enhances the evaporation/sublimation process. Diabatic cooling from melting and evaporation is most effective at levels below the melting level. Convergence within the downshear wake is thus instrumental in transporting precipitation into the downshear flank. Therefore, a comprehensive understanding of the downdraft initiation process is closely related to the precipitation initiation and transport process within clouds and is observable in passive MW imagery, as shown in the following case studies. Such processes depend not only on vertical profiles of temperature and moisture but also on vertical environmental wind profiles. Knupp (1996) identified the protrusion echo produced by settling hydrometeors from a line of weak updraft that formed in association with low-level confluence located east of the storm core. The protrusion

appeared to be partly forced by existing mesoscale convergence, while the updraft within its lower levels represented the weak low-level ascent along the up-down downdraft branch. In this regard, the protrusion was indirectly connected to the strong core downdraft. Initial bowing of the echo (Przybylinski 1995) was associated with the early microburst activity, a characteristic observed in other case studies. The inference of downburst occurrence can be successfully applied by the synergistic use of satellite-based passive MW and ground-based Doppler radar data and imagery.

From Weisman, Klemp, and Rotunno (1988) as a departure point, Weisman (1992) explored the role of vertical wind shear and buoyancy in the generation of a rear inflow jet and visualized the associated conceptual model of this process. Weisman (1992) noted that rear inflow is generated in response to the development of an upshear-tilted updraft, as the horizontal buoyancy gradients along the back edge of the expanding system create a circulation that draws midlevel air in from the rear. The rear inflow jet system can take two forms, descending and elevated. For a descending-jet system, the convective circulation is characterized by an updraft current that ascends gradually above a spreading surface cold pool, with light-to-moderate convective and stratiform rainfall extending well behind the leading edge of the cold pool. This structure is often associated with a decaying system. The gust-front lifting is not strong or deep enough to regenerate new convective cells, and the mesoscale circulation slowly weakens. However, for an elevated-jet system, the circulation is dominated by strong, erect updrafts along the leading edge of the surface cold pool, with the updraft current spreading rapidly rearward above 7-8 km above ground level. Moderate-to-heavy convective rainfall exists at the system's leading edge, with lighter

rainfall extending to the rear. This structure tends to be longer-lived than the descending-jet case, as the deeper gust-front lifting regularly regenerates strong convective cells. The rear-inflow jet represented a new, potentially significant horizontal vorticity source that must be included when diagnosing various circulation sources' relative importance. Specifically, a rear-inflow jet that descends and spreads along the surface is characterized by the same sign of horizontal vorticity generated by the cold pool, thereby accentuating the cold pool circulation.

In contrast to a descending jet, an elevated rear-inflow jet is characterized by the opposite sign of horizontal vorticity generated by the cold pool (up to jet level), thereby accentuating the ambient vertical shear effects. Since significant rear-inflow characteristically develops after the cold-pool circulation overwhelms the ambient shear, a surface jet's development reinforces the upshear-tilting process that tends to weaken the system. However, an elevated rear-inflow jet's development reverses this process, promoting powerful, upright convective cells along the cold pool's leading edge. Johns (1993) built on the basis established by previous observational and modeling studies of environmental conditions associated with the development and maintenance of bow echo-induced damaging winds, focused on parameters related to storm outflow and updraft strengths. Specifically, wind speeds and relative humidity values in the mid-levels (related to outflow strength) and instability (related to updraft strength) were examined. The results indicated that these parameters exhibit a wide range of values when considering all bow echo situations in which damaging winds are reported. Further, combinations of wind speeds in the mid-levels and instability tend to vary with the season and the synoptic situation. For example,

when powerful winds are present in the mid-levels, bow echo development has been observed in only marginally unstable environments. Bow echo events associated with the powerful wind-marginal instability combination typically occur with strong, rapidly moving low-pressure systems ("dynamic" synoptic pattern) in the colder months of the year. On the other hand, events associated with the relatively weak wind-extreme instability combination typically occur along a quasi-stationary thermal boundary in relatively stagnant weather regimes ("warm season" synoptic pattern) in the late spring or summer. Many bow echo wind events are associated with wind-instability combinations between the extremes. Some of these events are related to synoptic patterns that do not sufficiently match either prototypical pattern.

As will be demonstrated in the following case studies, passive microwave (MW) observations from polar-orbiting satellites are instrumental in identifying convective storms with dense ice-phase precipitation cores that can generate intense downdrafts by the processes of loading, melting, and evaporation. At a 12.5 km horizontal resolution, the 91 GHz channel on the Special Sensor Microwave Imager Sounder (SSMIS) effectively views the rainband structure in which both 91 GHz polarization (horizontal, "H," and vertical, "V") generate images where cirrus cloud decks are transparent. The SSMIS is a conical scanner with a 53.1° zenith angle, swath width 1700 km, scan rate of 31.9 scans/min, which equals 12.5 km/scan. Ferraro et al. (1998) introduced an expression to quantify brightness temperature derived from Schwarzchild's equation:

$$TB = T_u + \tau \cdot [\varepsilon \cdot T_s + (1 - \varepsilon) \cdot T_d] \quad (2)$$

Where T_u is upwelling atmospheric emission, τ is transmittance, ε is emissivity, T_s is surface temperature, and T_d is downwelling atmospheric emission. Scattering by large precipitation particles, especially by graupel, hail, and ice crystal aggregates (i.e., snow) above the freezing level, causes 91 GHz brightness temperatures (TB) to be low, referred to as a TB depression (Ferraro et al. (2015), Laviola et al. (2020)). Thus, convective rainbands tend to have very low TB, often below 200 K. Time trends in cloud top TB, as measured in MW spectrum window channels, and spatial patterns of cloud top TB, especially the geometry of TB gradients, can be exploited to infer downburst generation.

3 Field Measurement Application Methodology

Surface-based measurements in the radio and microwave regions of the electromagnetic spectrum provide important environmental parameters for monitoring atmospheric stability and mesoscale and microphysical processes associated with convective storm development. Over CONUS, traditional datasets applied to both operational downburst monitoring and prediction, as well as product validation, include surface-based observations of atmospheric parameters (i.e., temperature, humidity, wind speed/direction, sky condition, precipitation accumulation, etc.) from NWS/FAA aviation routine meteorological reports (METAR) stations, mesonetwork (mesonet) stations, radiosonde observations (RAOBs; see Chapter 2), and meteorological Doppler radar reflectivity and velocity measurements. The highest quality networks in CONUS include the Oklahoma Mesonet and West Texas Mesonet (Brock et al. 1995; Schroeder et al. 2005). These networks have a spatial density of weather stations suitable for observing patterns such as outflow boundaries and temperature perturbations resulting from convective storms. In

effect, surface weather observation and analysis represent a primary important step in convective storm diagnosis process.

An ultra-high frequency (UHF) Boundary Layer Profiler (BLP) is capable of identifying mesoscale features such as low-level jets, rear-inflow jets, and convective storm outflow and can supplement the Next Generation Weather Radar (NEXRAD) velocity azimuth display wind profile (VWP) product at longer distances (> 30 km) from the adjacent NEXRAD site. The BLP is a Doppler radar system operating at a frequency of 915 MHz that provides high-resolution observations with enhanced sensitivity to hydrometeors (Eklund et al. 1987) in which backscattered signals from turbulence-induced refractive index variations are detected by the radar (Martner et al. 1993). The BLP retrieves horizontal wind speed and direction up to an elevation of four kilometers above ground level at a vertical resolution of 60 m. In selected regions of CONUS, an expanded dataset incorporates lower tropospheric vertical wind profile data. For example, in this chapter we will utilize a BLP in Beltsville, Maryland (United States), which is near the capital, Washington DC. The BLP at Howard University Beltsville Campus (HUBC) provides the most representative wind conditions in the Washington, DC metropolitan area. These BLPs are component of the Cooperative Agency Profilers (CAP) network, which compiles data in real-time, applies quality control, and distributes the data online. Current and archived BLP wind data is available on the CAP website: https://madis-data.ncep.noaa.gov/cap/

In addition, vertical temperature and moisture sounding datasets generated by the surface-based microwave radiometer profiler (MWRP) provide routine monitoring of

thermodynamic patterns in both the pre-convective and storm environments (Westwater et al. 2005). In the Washington, DC – Baltimore, Maryland corridor, the HUBC MWRP, manufactured by Radiometrics Corporation, observes atmospheric brightness temperatures in 12 frequency bands from 22 to 59 GHz and retrieves temperature and humidity soundings up to 10 km height with a vertical resolution of 50 m below 500 m AGL and a resolution of 100 m between 500 and 2000 m AGL. The MWRP exploits the 30 to 50 GHz transmission window to retrieve water vapor profiles, while exploiting the absorption band near 60 GHz for temperature sensing. The HUBC MWRP employs the neural network (NN) inversion method of retrieval, trained with a large dataset of profiles generated from historical datasets of operational radiosondes. Vertical temperature and humidity profiles are often applied to calculate CAPE. This chapter will demonstrate the thunderstorm downburst potential applications of the microburst windspeed potential index (MWPI, Pryor 2015) as calculated from MWRP and satellite sounding datasets.

In the next section, we present two case studies, one for April 2020 in South Texas and another the June 2012 North American Derecho. These studies were selected because they (1) demonstrate the physical process of downburst generation described in Section 2 and they were (2) observed simultaneously by the microwave sensors onboard polar-orbiting meteorological satellites, vertical sounding profiles generated from the Infrared Atmospheric Sounding Interferometer (IASI) and the NOAA Unique Combined Atmospheric Processing System (NUCAPS), NEXRAD, and BLPs. NUCAPS (Nalli et al. 2020) is a NOAA enterprise algorithm that retrieves atmospheric profile environmental data records and is described in more detail in chapters 14 and 18. The IASI instrument

and its applications for vertical atmospheric sounding are also highlighted in chapter 18. Data collection, processing, and visualization follow the methodology of Pryor (2015, 2017). We use microwave sensors on Meteorological Operational (METOP) and Defense Meteorological Satellite Program (DMSP) satellites. DMSP Special Sensor Microwave Imager Sounder (SSMIS) and METOP Microwave Humidity Sounder (MHS) 89-91 GHz window channel datasets were obtained from the NOAA Comprehensive Large Array-data Stewardship System (CLASS) and the EUMETSAT Data Centre, respectively. Dual-polarized 91 GHz brightness temperature datasets allow for the calculation of polarization-corrected temperature (Liu et al. 1995) as presented in the study of the April 2020 South Texas downburst case. Vertical temperature and wind profile data, up to 5 km above ground level, from the CAP network are applied to further study the favorable environment for severe convective storm winds.

The Next Generation Weather Radar (NEXRAD) level-II reflectivity and differential reflectivity factor ZDR are obtained from the National Center for Environmental Information (NCEI) and used to verify that observed wind gusts are associated with downbursts originating from high reflectivity factor storms and are not associated with other types of convective wind phenomena (i.e., gust fronts). Plan-view images of radar reflectivity and ZDR are constructed from the lowest elevation angle scan (0.46°). An additional application of radar reflectivity factor imagery is to infer microscale physical properties of downburst-producing convective storms. Differential reflectivity factor is employed in case studies to analyze the vertical precipitation composition in convective storms and thereby indicate the presence of graupel and hail and discuss their role in the

enhancement of convective downdrafts. Particular reflectivity signatures, such as bow echoes (Przybylinski 1995) and protrusion echoes (Knupp 1996), are effective indicators of downburst occurrence. Downburst occurrence can be further confirmed by calculating a surface ΔT value, where $\Delta T \equiv T(\text{downburst}) - T(\text{ambient})$ and represents the peak temperature departure from ambient at ground level (Proctor 1989). ΔT can therefore serve as a proxy variable for the surface density perturbation through the ideal gas law. In summary, a comprehensive approach of observational data analysis involves both surface- and satellite-based instrumentation. Because this approach utilizes operational products available to weather service forecasters, it can feasibly be used for monitoring and forecasting downburst occurrence. Compared to other ground-based microwave imagery sources, such as Doppler radar, spatial patterns in TB can also infer airflow characteristics and circulation patterns surrounding the convective storm of interest.

4 Case Studies of Field Measurement Applications

4.1 27 April 2020 South Texas Severe Thunderstorm Downbursts

A cluster of thunderstorms developed west of the dryline over the Davis Mountains of southwestern Texas during the afternoon of 27 April 2020, while a dryline extended from east of Midland, Texas to the Big Bend area as shown in the 2100 UTC surface analysis in Figure 2. The thunderstorm cluster then merged to form an intense MCS with a leading bow echo (not shown) near the westward bulge in the dryline. As noted by Schaefer (1986) and Ziegler et al. (1997), the dryline is often a focus of differential heating, boundary layer convergence, and solenoidal circulation with an attendant release of instability and convective storm intensification. After dryline interaction, the MCS tracked rapidly

southeastward toward the Gulf Coastal Plain. Figure 3a shows a mid-afternoon (1946 UTC) NUCAPS physical retrieval sounding profile over Del Rio, Texas, which can be compared to a RAOB released from the same location four hours later, at 0000 UTC on 28 April (Figure 3b). The earlier NUCAPS Skew-T diagram (Figure 3a) shows considerable CAPE (> 4000 J/kg), a large lower tropospheric temperature lapse rate (> 9° C/km), and a prominent mid-tropospheric unsaturated layer. These features indicate an elevated probability of severe thunderstorm downburst occurrence, roughly six hours before the onset of the severe windstorm. A MWPI value of 6.9 indicated thunderstorm wind gust potential of 60 knots. MWPI values greater than 5 indicate a high probability of severe winds greater than 50 knots in magnitude. In addition, the corresponding equivalent potential temperature (theta-e) profile signified potential instability with a decreasing value from the surface upward to a minimum in the middle troposphere. The calculated surface to 500 mb theta-e difference of 29°K (Figure 3c and 3) significantly exceeds the 20°K threshold for downburst occurrence as documented by Atkins and Wakimoto (1991). Comparing the 1945 UTC (2:45 pm local time) NUCAPS sounding profile (Figure 3a), to the 0000 UTC (7:00 pm local time) 28 April RAOB from Del Rio (Figure 3b), with a distance between retrieval locations of 22 km (12 n mi), shows that the risk for severe weather persisted into the evening.

Previous evaluations of NUCAPS for stability index calculation and convective weather forecasting applications (Bloch et al. 2019; Esmaili et al. 2020) described the necessity and resultant implementation of a modification technique to mitigate temperature and moisture biases in the boundary layer. This boundary layer correction replaces NUCAPS surface temperature and dewpoint temperature measurements with adjacent data from the Real

Time Mesoscale Analysis (RTMA). The modification technique for the NUCAPS sounding profile in this case study, as shown in Figure 4, was applied by adding the surface temperature and dew point measurements from Del Rio International Airport (DRT) to the retrieval. This procedure resulted in a stronger signal for severe outflow wind generation as evidenced by increased wind gust potential to 65 knots. Accordingly, the National Weather Service/Storm Prediction Center, in mesoscale discussion (MCD) #0481 issued at 2333 UTC 27 April, placed the Del Rio area in the southeastern periphery of a threat region for isolated strong/severe wind gusts (Figure 5a). A Laughlin AFB NEXRAD reflectivity image highlighted the linear structure of the MCS with an array of protrusion echoes pointing downshear (Figure 5b). This MCS likely generated a downburst cluster, resulting in wind gusts of 67 and 65 knots, recorded at Del Rio International Airport at 0135 UTC and at Laughlin Air Force Base at 0150 UTC 28 April, respectively. Calculated gust factors near 1.6 and ΔT values of -12 to -13°C for both wind events are consistent with downburst occurrence (Choi and Hidayat 2002, Proctor 1989).

Defense Meteorological Satellite Program (DMSP) F-17 and MetOP-A overpasses were optimal for retrieving cloud microphysical properties before and shortly after the downburst in the Del Rio area, as inferred from TB measurements shown in Figure 6. Imagery from Special Sensor Microwave Imager Sounder (SSMIS) and Microwave Humidity Sounder (MHS) displayed in Figure 6 show remarkably cold cloud tops (white shading) and large graupel water path values (> 1 mm) that indicated significant storm severity. As shown in Figures 6a and 6b, the 91 GHz channel is an atmospheric window in the microwave spectrum. Scattering by ice-phase precipitation particles, especially graupel, hail, and snow above the freezing level causes the TB depression (Ferraro et al.

2015, Laviola et al. 2020) around the time of peak storm intensity. For this case, TB near the storm centroid was remarkably low (~120 K) and corresponded to a maximum in graupel water path (GWP) values (> 10 mm), indicating the presence of a dense core of graupel/hail. A large ice content and prominent dry-air notches on the lateral and downshear (forward) flanks of the storm indicated favorability for strong thunderstorm downdraft generation (Srivastava 1987, Knupp 1989). MetOP-A MHS imagery shown in Figures 6c and 6d displayed remarkably cold cloud tops (white shading) and large graupel water path values (> 1 mm) that indicated significant storm severity.

This intensive study of a severe convective wind event demonstrates the value of a synergistic analysis of satellite and ground-based sensor data. This is illustrated by the afternoon NUCAPS vertical profile pointing to the potential for convection and verification by the appearance of severe convective storms in SSMIS and MHS imagery. Successive overpasses of DMSP F-17 and EPS MetOP-A satellites shown in Figure 7 provided microwave imagery that effectively visualized the severe MCS evolution. Figure 8 demonstrates the application of brightness temperature differencing to more effectively extract signatures associated with storm severity and intense convective downdraft generation. A new algorithm is the differential brightness temperature (BTDR) between the horizontal and vertical polarization channels that is analogous to Doppler radar-derived differential reflectivity:

$$BTDR = 100*(\log_{10}(TB91_H/TB91_V)) \quad (3)$$

where $TB91_H$ and $TB91_V$ represent horizontally and vertically polarized 91 GHz brightness temperatures, respectively. Small negative values of SSMIS-derived BTDR correspond to

large graupel water path values (> 10 mm), and thus, to a mixture of rain, hail, and graupel. The calculation of BTDR is compared to the established polarization corrected temperature (PCT, Spencer et al. (1989)), defined as:

$$PCT = (1.818*TB_V) - (0.818*TB_H) \quad (4)$$

where TB_H and TB_V represent horizontally and vertically polarized brightness temperatures, respectively. PCT values below 200K typically correspond to high precipitation rates and large ice-phase precipitation content.

As shown in Figure 9, the velocity azimuth display (VAD) wind profile (VWP) from Laughlin Air Force Base (AFB) NEXRAD, this multicellular storm tracked east-southeastward with weak low-level shear that was nearly parallel to the storm line, which allowed for a short episode of severe downburst winds over the Del Rio area, followed by gradual weakening of the system and cessation of severe winds. Also apparent were inward-directed V-shaped TB gradients on the downwind (eastern) flank of the storm that suggests the occurrence of wake entrainment of sub-saturated air and subsequent downdraft acceleration by the process detailed in Knupp (1989). The absence of an apparent rear-inflow jet was likely a factor in the episodic and short-lived occurrence of downburst winds at Del Rio with a duration only 15 minutes, from 0135 to 0150 UTC 28 April. However, these storms still produced significant structural damage and power outages on a local scale.

4.2 29 June 2012 North American Derecho

During the morning of 29 June 2012, an area of convective storms over Iowa organized into a quasi-linear convective system (QLCS) as it tracked into northern Illinois. The system then evolved into a bow echo (Przybylinski 1995) during the afternoon and tracked southeastward over the Ohio Valley to the Mid-Atlantic coast by late evening. What would eventually become the 29 June 2012 North American Derecho, this QLCS produced its first significant severe downburst, with winds measured over 65 knots, at Michigan City, Indiana during the early afternoon. This extraordinary derecho-producing convective system (DCS) event resulted in 22 deaths and nearly a thousand severe wind reports from northern Illinois to the Atlantic Coast. This system was more typical of a warm-season progressive derecho, as shown in Figure 10, associated with a major heat wave and an elevated mixed layer (Banacos and Ekster (2010)). This DCS was generated and then propagated within a mid-tropospheric ridge synoptic pattern as identified by Johns (1993) and Coniglio et al. (2004). During the evening of 29 June, the derecho tracked rapidly eastward across the mountains of West Virginia (WV), western Virginia (VA), southwest Pennsylvania (PA), and western Maryland (MD) during mid-evening. The derecho's effects were particularly formidable in the Washington, DC – Baltimore, MD corridor, where measured wind gusts of 60-70 knots severed numerous overhead electrical feeders.

Comparison of the late evening MetOP-A Infrared Atmospheric Sounding Interferometer (IASI) sounding near Salisbury, Maryland to the HUBC microwave radiometer (MWR) sounding at 0200 UTC 30 June in Figures 11 and 12, exhibits a transition to a moist and highly unstable profile favorable for severe wet microbursts. Figure 11 illustrates the sounding modification process to further enhance the signal for severe deep convective

storm development. In Figure 11a, the IASI thermodynamic profile indicated modest convective storm potential. Incorporating the 0154 UTC surface temperature and dew point observation from Salisbury Regional Airport (27 km (14 n mi) north of the IASI retrieval site), as shown in Figure 11b, results in significantly larger CAPE. Finally, substituting the dry bulb temperature dataset with calculated virtual temperature yields the strongest signal for severe downburst generation with wind gust potential of 57 knots, comparable to the potential derived from the HUBC MWR sounding as demonstrated in Figures 11c and 12. Accordingly, the MWPI increased in magnitude prior to the onset of the derecho to eventually indicate convective wind gust potential of 55-57 knots with an hour of lead time. Between 0000 and 0200 UTC, as shown in Figure 13, the DCS evolved into a double-bow echo pattern with a "warm advection wing" (Smith 1990) over Frederick County (near latitude 39.5°N/longitude 77.4°W) that developed in an east-west oriented region of weak surface convergence over central Maryland.

Figure 13 exhibits a type 2 derecho echo pattern with a warm advection wing (Przybylinski 1995) that extended downwind (eastward) from the northern end of the bulging line echo. Microbursts occurred in Frederick County within the warm advection wing of the derecho. MetOP-A MHS, with overlying Sterling, VA (LWX) NEXRAD reflectivity, revealed the presence of the warm advection wing. A dry air notch, displayed as an inward (eastward) pointing TB gradient, likely indicated the presence of a rear-inflow jet ("RIJ") that sustained the MCS and the generation of downburst clusters in the DC-Baltimore corridor during the following hour. A shown in Figures 14 and 15, the RIJ was apparent and distinguishable from surface-based outflow in the Sterling, Virginia NEXRAD VWP and Beltsville, Maryland 915 MHz Boundary Layer Profiler (BLP) wind observation time

series, respectively. Near 0250 UTC, a downburst cluster tracking over downtown Washington, DC produced measured wind gusts of 61 and 47 knots at Reagan National Airport and the Washington Physical Oceanographic Real-Time System (PORTS) station, respectively. A gust factor of 1.42 and ΔT values of -10 to -11°C were also consistent with downburst occurrence embedded in the larger-scale DCS.

In retrospect, NWS/Storm Prediction Center (SPC) adequately indicated the likelihood of scattered severe winds over the Washington, DC – Baltimore, MD corridor as the derecho tracked east of the Appalachian Mountains during the late evening. However, the density and magnitude of severe wind events, and associated impacts, over the Washington, DC metropolitan area, including the adjacent Maryland and Virginia suburbs, was not anticipated by neither SPC nor the NWS Office Baltimore-Washington. Thus, science value added with this case study entails the application of evening NUCAPS sounding profiles and derived parameters that will provide more insight to the evolution of the nocturnal convective lower troposphere. MW window channel data will more effectively interrogate evolving DCSs and reveal greater detail of storm structure, especially pertaining to convective wind generation. An important outcome of this study will be to formulate a correlation between MW parameters and signatures, and severe convective wind occurrence.

5 Summary

Convective storm-generated downbursts are an operational forecasting challenge due to the spectrum of time, space, and intensity scales in which they occur. This chapter assembled the governing physical theory essential for development of downburst

prediction algorithms that proceeds from vertical momentum equations and the aggregate of thermodynamical and microphysical processes of precipitation. Accordingly, downburst monitoring and subsequent prediction is a three-step process with an objective to build a three-dimensional model of the thermodynamic structure of the ambient environment and conceptual model of downburst-producing convective storms:

1. Collection and exploitation of surface-based observations including measurements from tower platforms and Doppler radar-measured reflectivity and wind velocity.
2. Ground-based microwave and radio profiler instruments, including MWRPs and BLPs, to obtain vertical profiles of temperature, humidity, and wind velocity.
3. Satellite-based 2-D plan view images of brightness temperature and vertical profiles of temperature and humidity. Modification of sounding profiles with surface observations of temperature and humidity is an additional step that results in improved representation of the ambient environment.

The case studies demonstrate how both ground-based and satellite-based observational data for convective storms can be combined for monitoring and forecasting applications. Field measurements are the cornerstone for remote sensing techniques and are essential for understanding deep convective storms and associated downburst occurrence, phenomena that encompass the vertical dimension of the troposphere.

Figures

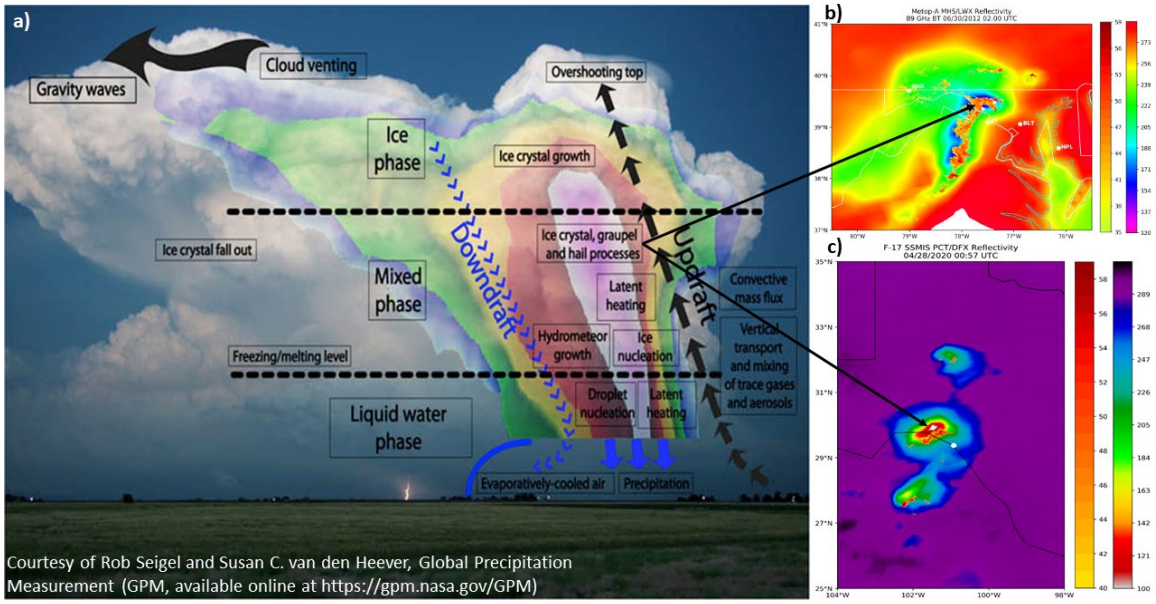

Figure 1. (a) Conceptual model of a deep convective storm; (b-c) microwave imagery examples from downburst events that occurred during the past decade demonstrate an improvement in the inference of storm structural characteristics.

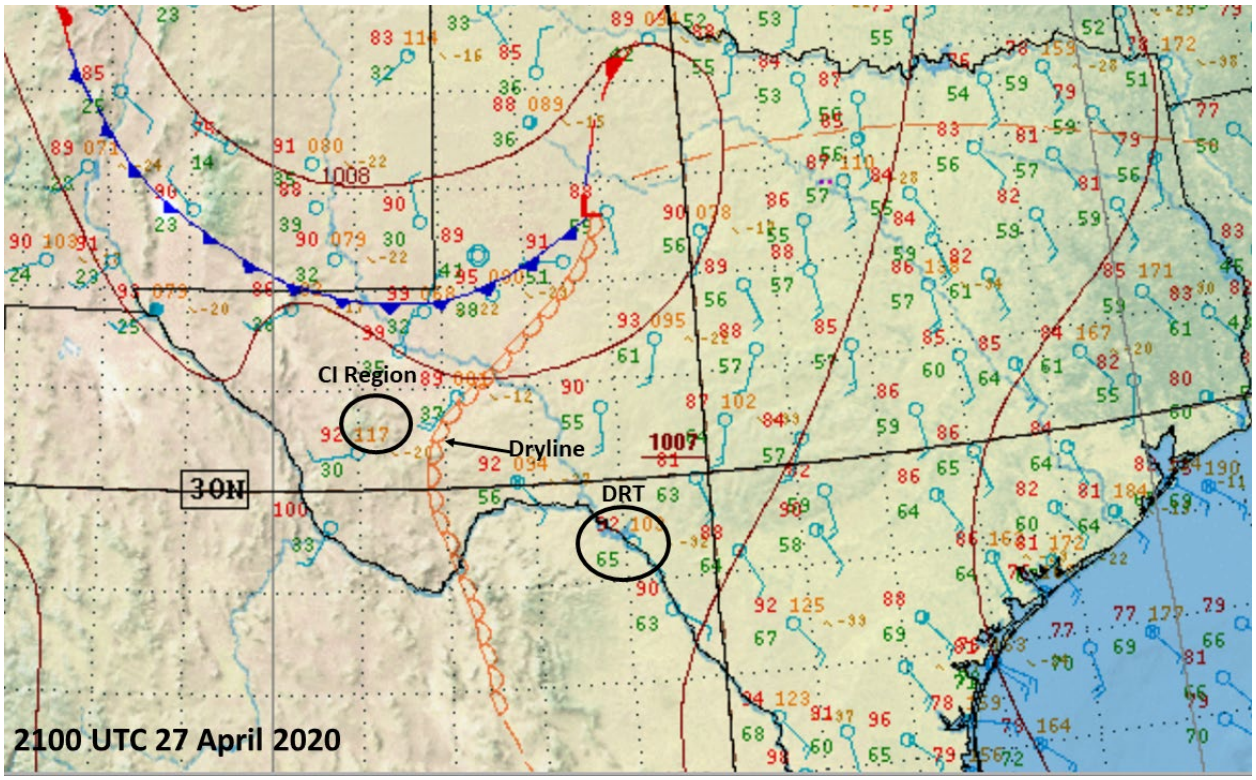

Figure 2. Surface analysis over the southern Great Plains region at 2100 UTC 27 April 2020. The black circled region labeled "DRT" represents the location of the Del Rio, Texas and the location of the NOAA-20 sounding retrieval. "CI" represents the convective initiation region over the Davis Mountains of Texas. Courtesy of NOAA/National Weather Service/Weather Prediction Center.

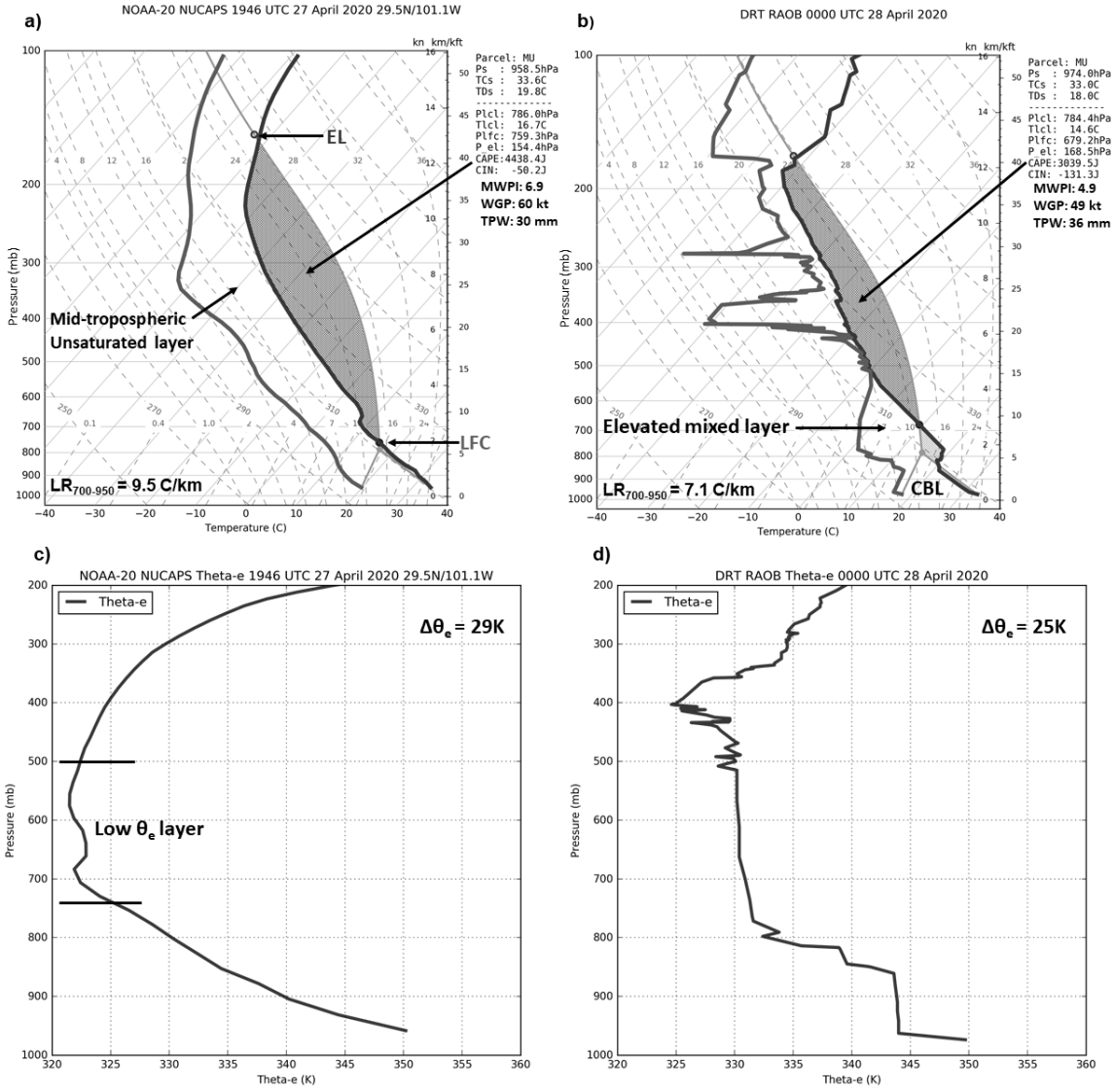

Figure 3. (a) A NOAA-20 NUCAPS sounding profile retrieved during the afternoon of 27 April 2020 as compared to (b) a radiosonde observation at Del Rio, Texas (DRT) at 0000 UTC 28 April 2020; (c) A NOAA-20 NUCAPS theta-e profile retrieved during the afternoon of 27 April 2020 as compared to (d) a radiosonde observation theta-e profile at Del Rio, Texas (DRT) at 0000 UTC 28 April 2020.

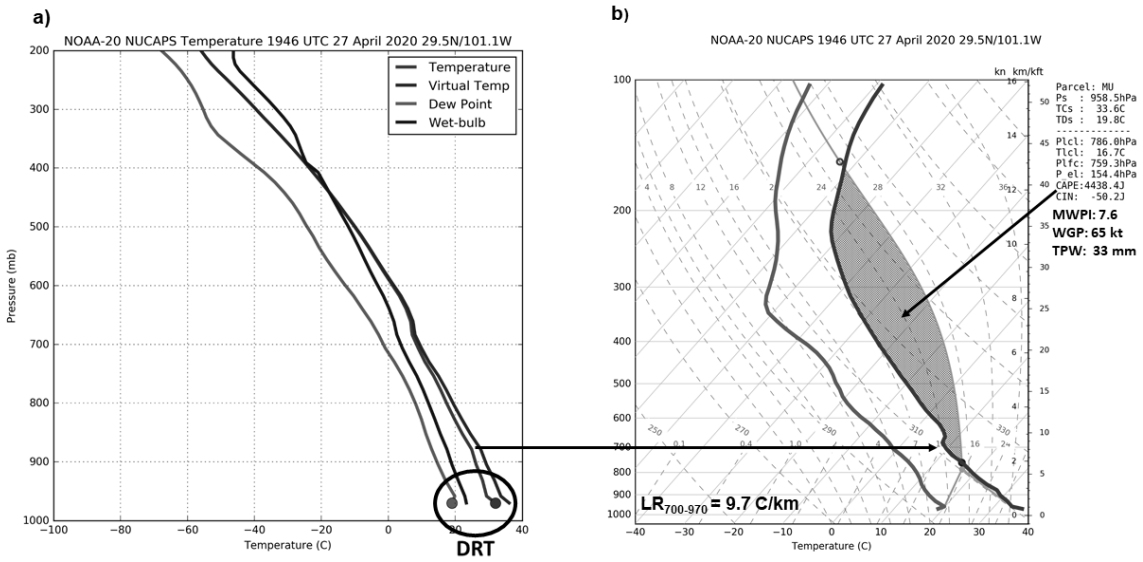

Figure 4. (a) The NOAA-20 NUCAPS temperature sounding profile marked with surface observations of temperature and dew point retrieved at 1946 UTC near Del Rio, Texas (DRT); (b) corresponding sounding profile over Del Rio modified with the surface temperature and dew point observations at DRT.

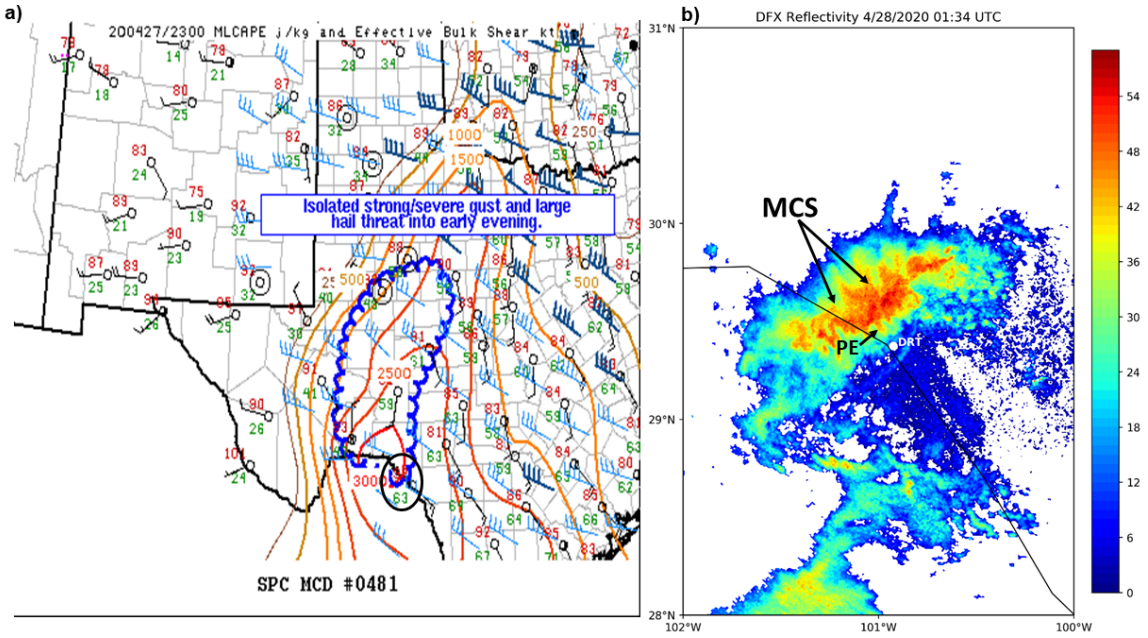

Figure 5. (a) NWS/SPC mesoscale convective discussion (MCD) at 2300 UTC 27 April 2020; (b) Laughlin AFB, Texas NEXRAD reflectivity at 0134 UTC 28 April 2020. Black-

circled region in (a) marks the location of Del Rio. “PE” represents the location of a protrusion echo.

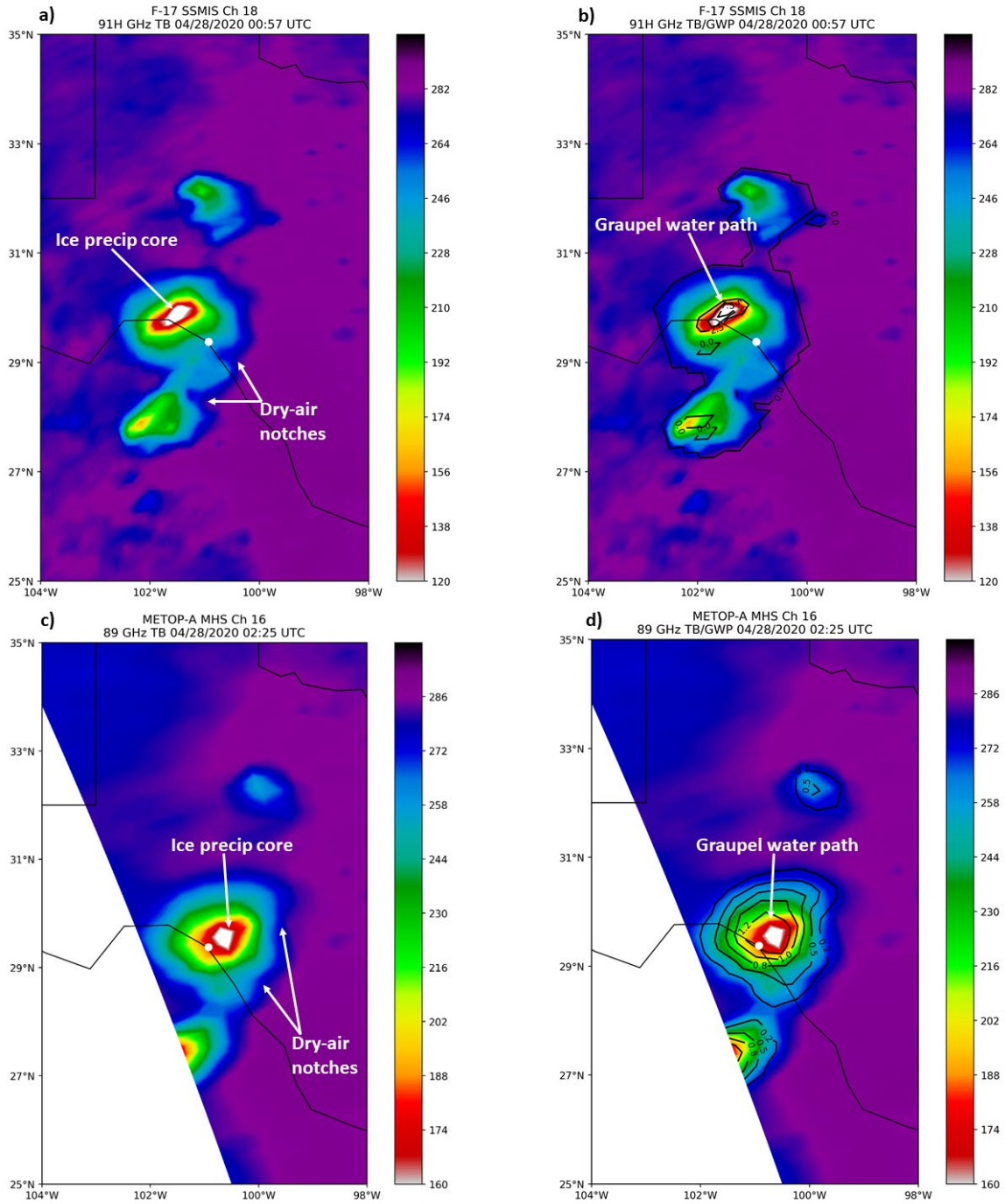

Figure 6. South Texas Regional F-17 SSMIS (a) 91 GHz brightness temperature image at 0057 UTC 28 April 2020 with (b) overlying graupel water path measurements; (c) MetOP-A Microwave Humidity Sounder (MHS) 89 GHz brightness temperature image at 0225 UTC 28 April 2020 with (d) overlying graupel water path measurements.

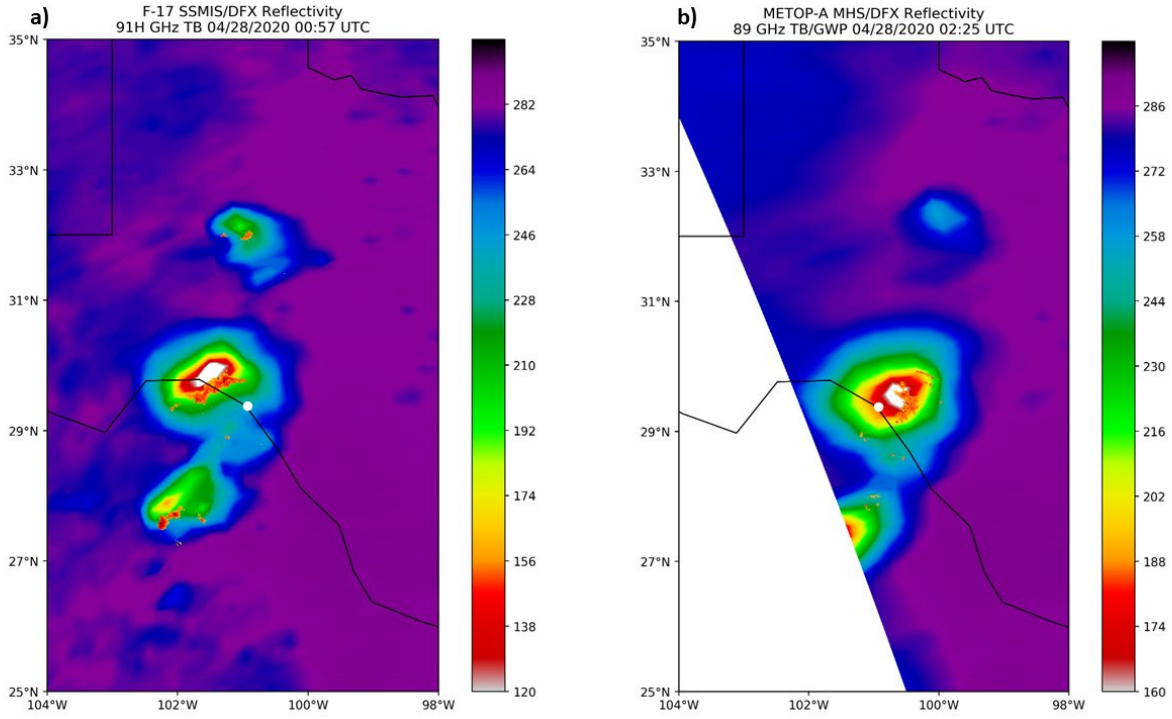

Figure 7. South Texas Regional F-17 SSMIS (a) 91 GHz brightness temperature image at 0057 UTC 28 April 2020 and (b) MetOP-A MHS 89 GHz brightness temperature image at 0225 UTC 28 April 2020 with overlying NEXRAD reflectivity measurements.

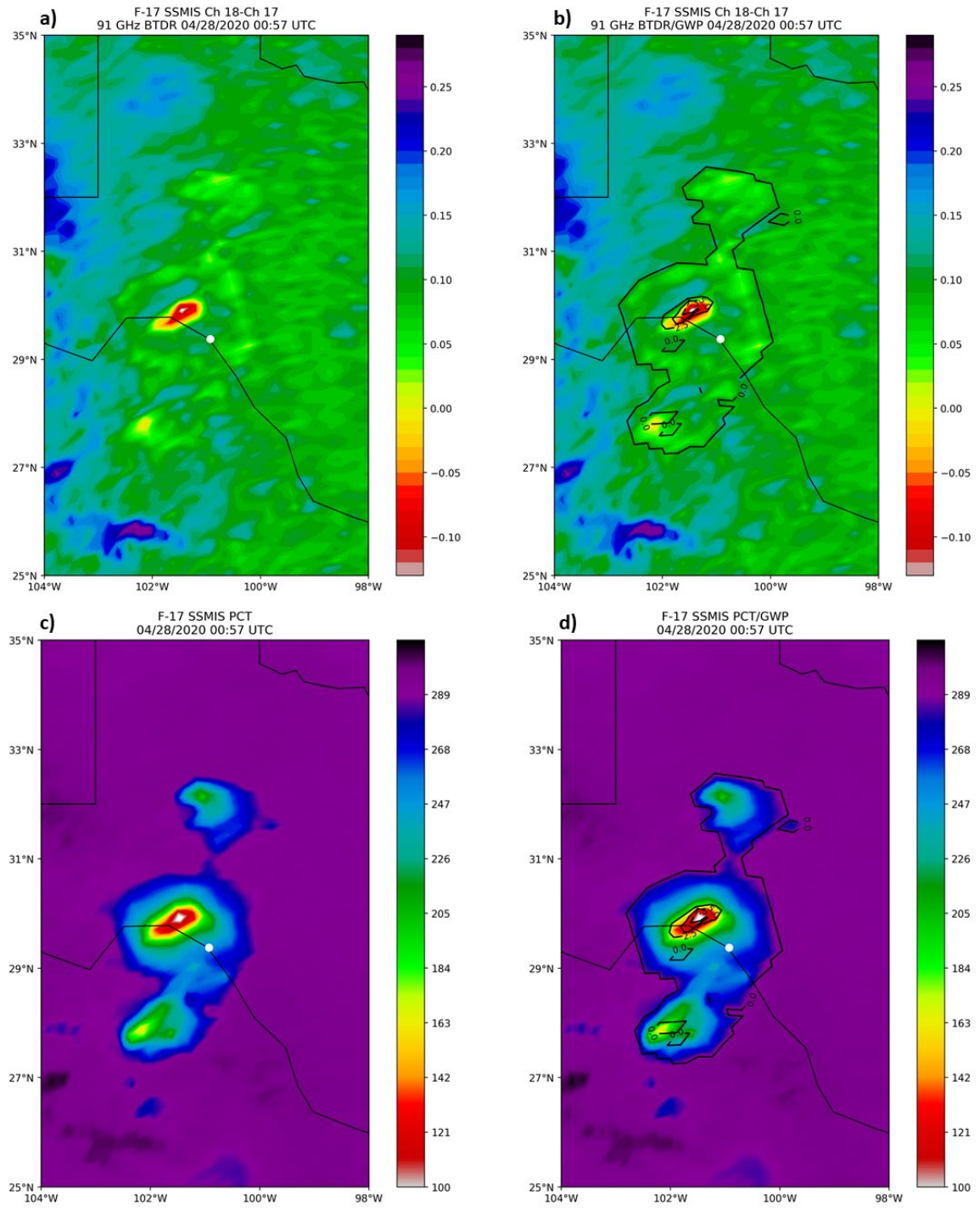

Figure 8. F-17 SSMIS (a) differential brightness temperature (BTDR) imagery and (c) polarization corrected temperature (PCT) near 0100 UTC 28 April 2020. (b) and (d) display the product imagery with overlying graupel water path measurements.

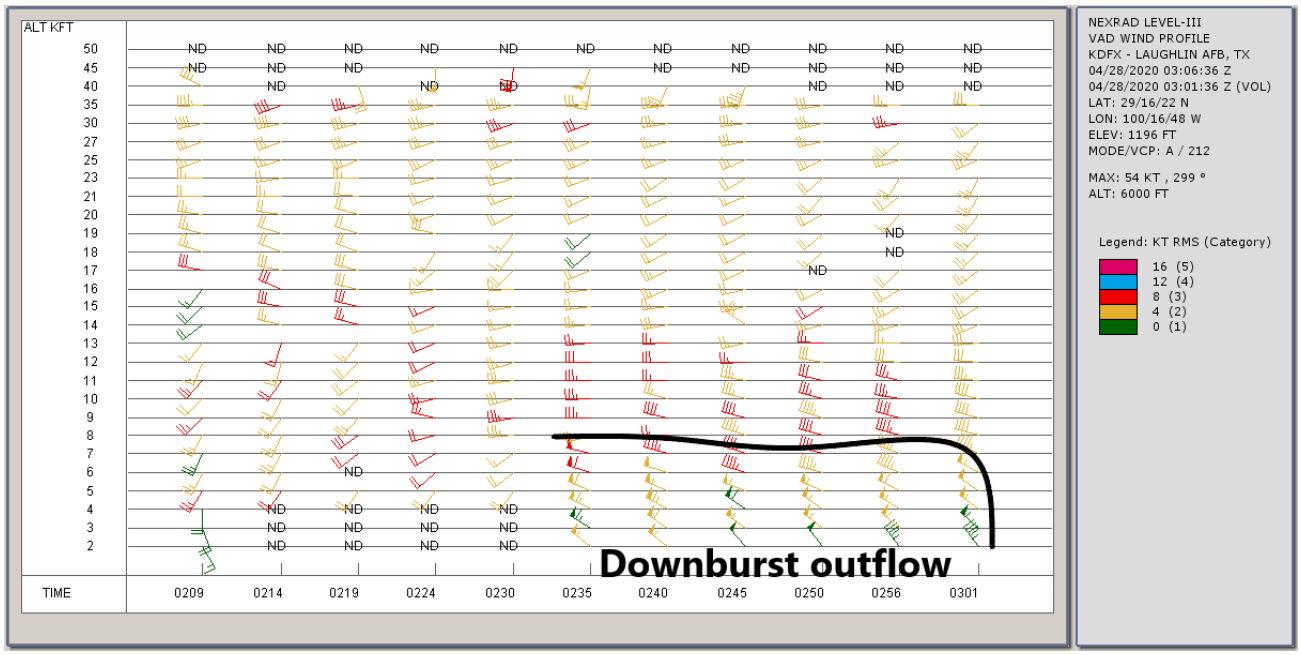

Figure 9. Velocity azimuth display (VAD) wind profile (VWP) from Laughlin Air Force Base (AFB) NEXRAD, near Del Rio, Texas between 0200 and 0300 UTC 28 April 2020.

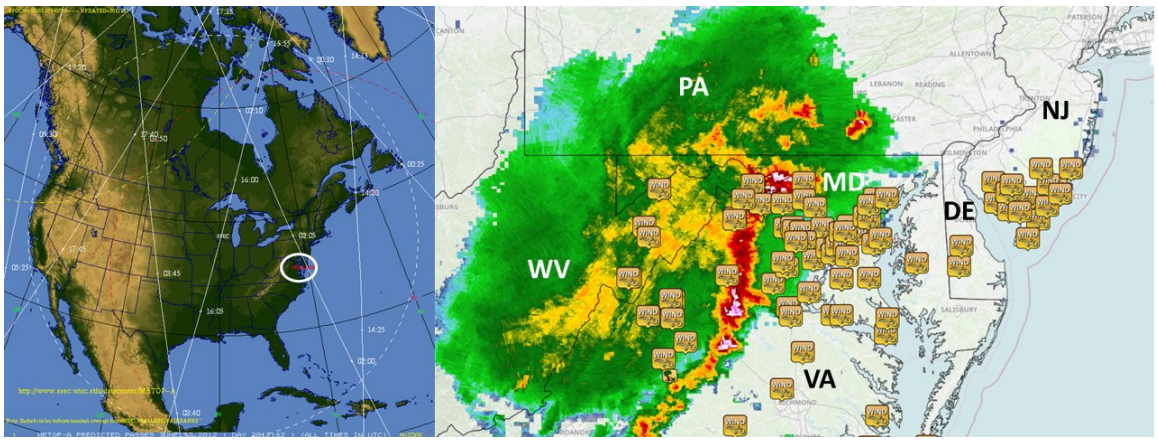

Figure 10. Map-view plot (right) of severe wind reports over the Mid-Atlantic region associated with the re-intensification phase of the derecho during the evening of 29 June 2012. White oval outline marks the location of the Metop-A overpass (left) over the Mid-Atlantic region between 0200 and 0205 UTC 30 June 2012 just prior to onset in the Baltimore, Maryland – Washington, DC metropolitan area. The states impacted by the

derecho are labelled: Delaware (DE), Maryland (MD), New Jersey (NJ), Pennsylvania (PA), Virginia (VA), and West Virginia (WV).

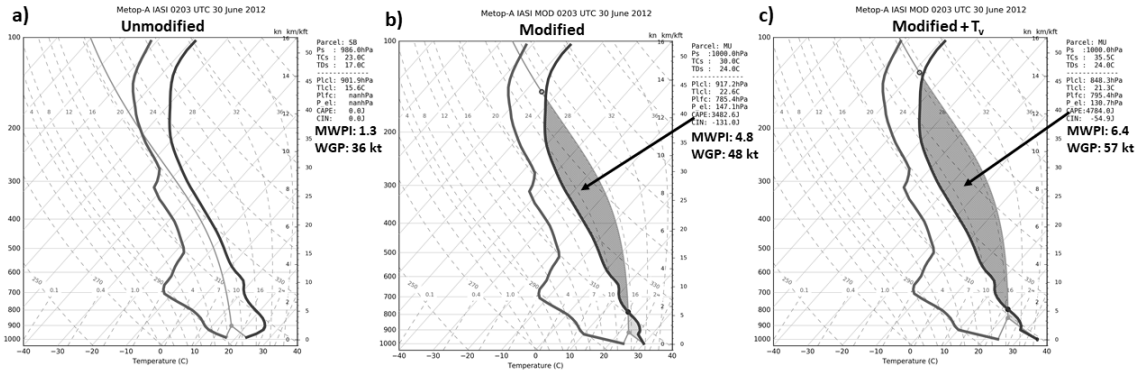

Figure 11. MetOP-A IASI retrievals near Salisbury, Maryland during the evening of 29 June 2012 (0203 UTC 30 June): (a) IR+MW sounding profile; (b) IR+MW sounding profile modified by observed surface temperature and dew point at Salisbury Regional Airport; (c) modified IR+MW sounding profile plotted with virtual temperature.

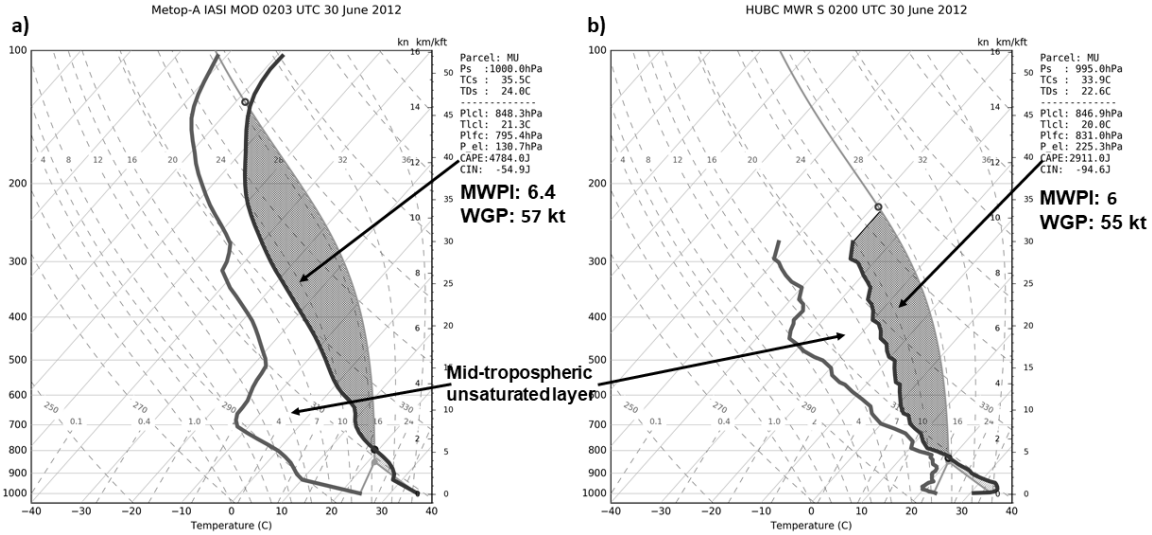

Figure 12. (a) Modified MetOP-A IASI IR+MW sounding profile retrieved near Salisbury, Maryland at 0203 UTC 30 June 2012 as compared to (b) a ground-based sounding profile retrieval from the Howard University, Beltsville, Maryland (HUBC) microwave radiometer (MWR).

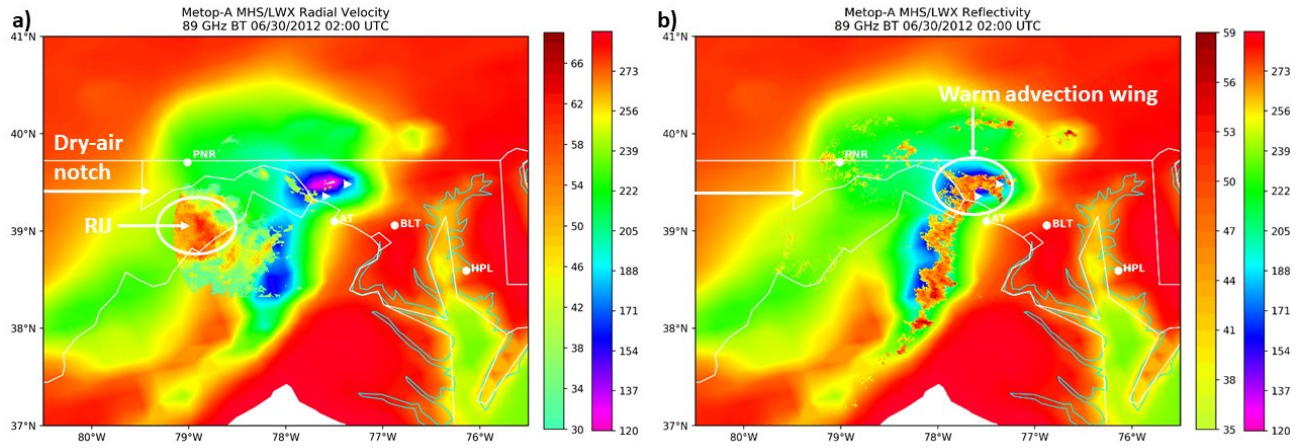

Figure 13. MetOP-A MHS 89 GHz brightness temperature image at 0200 UTC 30 June 2012 with (a) overlying NEXRAD radial velocity and (b) reflectivity measurements.

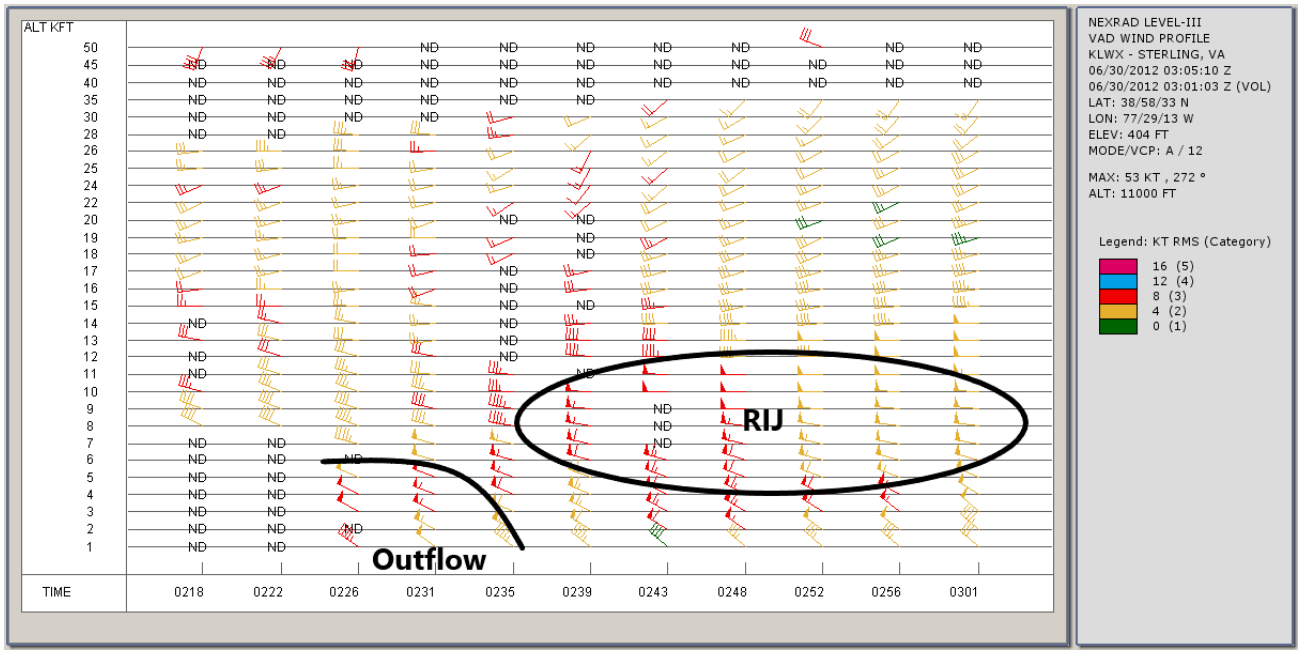

Figure 14. Velocity azimuth display (VAD) wind profile (VWP) from Sterling, Virginia NEXRAD between 0200 and 0300 UTC 30 June 2012.

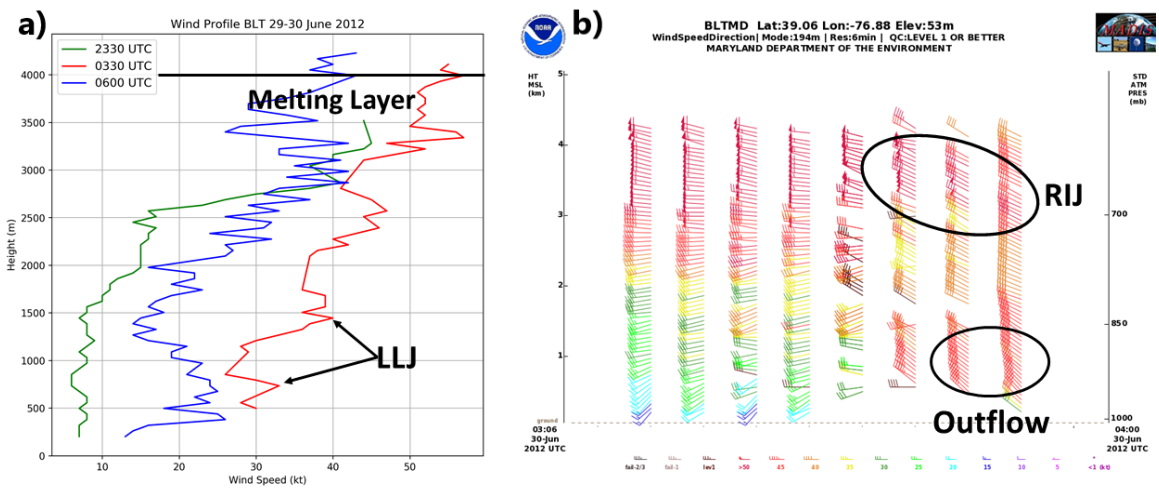

Figure 15. Time series of HUBC 915 MHz Boundary Layer Profiler (BLP) a) wind speed vs height (meters) between 2330 UTC 29 June and 0600 UTC 30 June 2012 and b) wind speed and direction vs height between 0300 and 0400 UTC 30 June 2012.

Bibliography

Ashley, W. S., and T. L. Mote, 2005: Derecho Hazards in the United States. Bull. Amer. Meteor. Soc., 86, 1577–1592.

Atkins, N. T., and R. M. Wakimoto, 1991: Wet microburst activity over the southeastern United States: Implications for forecasting. Wea. Forecasting, 6, 470–482.

Banacos, P.C., and M.L. Ekster, 2010: The association of the elevated mixed layer with significant severe weather events in the Northeastern United States. Wea. Forecasting, 25, 1082-1102.

Bloch, C.; Knuteson, R.O.; Gambacorta, A.; Nalli, N.R.; Gartzke, J.; Zhou, L. Near-Real-Time Surface-Based CAPE from Merged Hyperspectral IR Satellite Sounder and Surface Meteorological Station Data. J. Appl. Meteor. Clim. **2019**, 58, 1613–1632.

Brock, F. V., K.C.Crawford, R. L. Elliott, G.W. Cuperus, S. J. Stadler, H. L. Johnson, and M. D. Eilts, 1995: The Oklahoma Mesonet: A technical overview. J. Atmos. Oceanic Technol., 12, 5–19.

Choi, E. C., and F.A. Hidayat, 2002: Gust factors for thunderstorm and non-thunderstorm winds. *Journal of wind engineering and industrial aerodynamics*, *90*(12-15), 1683-1696.

Cimini, D., M. Nelson, J. Güldner, and R. Ware, 2015: Forecast indices from a ground-based microwave radiometer for operational meteorology. Atmospheric Measurement Techniques, 8(1), 315-333.

Coniglio, M. C., D. J. Stensrud, and M. B. Richman, 2004: An observational study of derecho-producing convective systems. Wea. Forecasting, 19, 320-337.

Ecklund, W. L., D.A. Carter, and B.B. Balsley, 1988: A UHF wind profiler for the boundary layer: Brief description and initial results. *Journal of Atmospheric and Oceanic Technology*, *5*(3), 432-441.

Ellrod,G. P., 1989: Environmental conditions associated with the Dallas microburst storm determined from satellite soundings. Wea. Forecasting, 4, 469–484.

Esmaili, R.B.; Smith, N.; Berndt, E.B.; Dostalek, J.F.; Kahn, B.H.; White, K.; Barnet, C.D.; Sjoberg, W.; Goldberg, M. Adapting Satellite Soundings for Operational Forecasting within the Hazardous Weather Testbed. *Remote Sens.* **2020**, *12*, 886. https://doi.org/10.3390/rs12050886

Ferraro, R.R., Kusselson, S.J. and Colton, M., 1998: An introduction to passive microwave remote sensing and its applications to meteorological analysis and forecasting. National Weather Digest, 22, 11-23.

Ferraro, R., Beauchamp, J., Cecil, D., and Heymsfield, G., 2015: A prototype hail detection algorithm and hail climatology developed with the Advanced Microwave Sounding Unit (AMSU). Atmospheric Research, 163, 24-35.

Fujita, T. T., 1985: The downburst, microburst and macroburst. Satellite and Mesometeorology Research Paper 210, University of Chicago, 122 pp.

Fujita, T. T., and R. M. Wakimoto, 1981: Five scales of airflow associated with a series of downbursts on 16 July 1980. Mon. Wea. Rev.,109, 1438-1456.

Johns, R. H. 1993: Meteorological conditions associated with bow echo development in convective storms. Wea. Forecasting, 8, 294-299.

Knupp, K.R., 1989: Numerical simulation of low-level downdraft initiation within precipitating cumulonimbi: Some preliminary results. Mon. Wea. Rev., 117, 1517-1529.

Knupp, K. R., 1996: Structure and evolution of a long-lived, microburst producing storm. Mon.Wea. Rev., 124, 2785–2806.

Laviola, S., Levizzani, V., Ferraro, R. R., and Beauchamp, J., 2020: Hailstorm Detection by Satellite Microwave Radiometers. Remote Sensing, 12(4), 621.

Liu, G., J.A. Curry, and R.W. Sheu, 1995: Classification of clouds over the western equatorial Pacific Ocean using combined infrared and microwave satellite data. Journal of Geophysical Research: Atmospheres, 100(D7), 13811-13826.

Martner, B. E., D.B. Wuertz, B.B. Stankov, R.G. Strauch, E.R. Westwater, K.S. Gage, and W.F. Dabberdt, 1993: An evaluation of wind profiler, RASS, and microwave radiometer performance. Bulletin of the American Meteorological Society, 74(4), 599-614.

Nalli, N.R.; Tan, C.; Warner, J.; Divakarla, M.; Gambacorta, A.; Wilson, M.; Zhu, T.; Wang, T.; Wei, Z.; Pryor, K.; Kalluri, S.; Zhou, L.; Sweeney, C.; Baier, B.C.; McKain,

K.; Wunch, D.; Deutscher, N.M.; Hase, F.; Iraci, L.T.; Kivi, R.; Morino, I.; Notholt, J.; Ohyama, H.; Pollard, D.F.; Té, Y.; Velazco, V.A.; Warneke, T.; Sussmann, R.; Rettinger, M. Validation of Carbon Trace Gas Profile Retrievals from the NOAA-Unique Combined Atmospheric Processing System for the Cross-Track Infrared Sounder. *Remote Sens.* **2020**, *12*, 3245. https://doi.org/10.3390/rs12193245

Proctor, F.H., 1989: Numerical simulations of an isolated microburst. Part II: Sensitivity experiments. J. Atmos. Sci., 46, 2143-2165.

Pryor, K. L., 2015: Progress and Developments of Downburst Prediction Applications of GOES. *Wea. Forecasting*, **30**, 1182–1200, DOI: 10.1175/WAF-D-14-00106.1.

Pryor, K.L., 2017: Advances in downburst monitoring and prediction with GOES-16. In 17th conf. on mesoscale processes, San Diego, CA, Amer. Meteor. Soc., Paper No. 10.6.

Przybylinski, R.W., 1995: The bow echo. Observations, numerical simulations, and severe weather detection methods. Wea. Forecasting, 10, 203-218.

Schaefer, J. T., 1986: The Dryline. *Mesoscale Meteorology and Forecasting*, P. S. Ray, Ed., American Meteorological Society, 549-572.

Schroeder, J. L., W. S. Burgett, K. B. Haynie, I. Sonmez, G. D. Skwira, A. L. Doggett, and J. W. Lipe, 2005: The West Texas Mesonet: A technical overview. J. Atmos. Oceanic Technol., 22, 211–222

Smith, B. E., 1990: Mesoscale structure of a derecho-producing convective system: The southern Great Plains storms of May 4 1989. Preprints, 16th Conf on Severe Local Storms, Kananaskis Park, AB, Canada, Amer. Meteor. Soc., 428-433.

Smull, B. F., and R. A. Houze, Jr., 1987: Rear inflow in squall lines with trailing stratiform precipitation. Mon. Wea. Rev., 115, 2869-2889.

Spencer, R.W., H.M. Goodman, and R.E. Hood, 1989: Precipitation retrieval over land and ocean with the SSM/I: Identification and characteristics of the scattering signal. *Journal of Atmospheric and Oceanic Technology*, *6*(2), 254-273.

Srivastava, R.C., 1987: A model of intense downdrafts driven by the melting and evaporation of precipitation. J. Atmos. Sci., 44, 1752-1773.

Wakimoto, R. M., 1985: Forecasting dry microburst activity over the high plains. Mon. Wea. Rev., 113, 1131–1143.

Weisman, M. L., J.B. Klemp, and R. Rotunno, 1988: Structure and evolution of numerically simulated squall lines. J. Atmos. Sci., 45, 1990-2013.

Weisman, M. L., 1992: The role of convectively generated rear inflow jets in the evolution of long-lived mesoconvective systems. J. Atmos. Sci., 49, 1826–1847.

Westwater, E. R., S. Crewell, and C. Matzler, 2005: Surface-based microwave and millimeter wave radiometric remote sensing of the troposphere: A tutorial. IEEE Geoscience and Remote Sensing Society Newsletter, 134, 16-33.

Ziegler, C. L., T. J. Lee, and R. A. Pielke, 1997: Convective Initiation at the Dryline: A Modeling Study. Monthly Weather Review, 125, 1001-1026.